Theor Chem Acc (2011) 130:727–737
DOI 10.1007/s00214-011-1058-x

REGULAR ARTICLE

Alkali metal doping effect on static first hyperpolarizabilities of PMI chains

Ling Zhi Kang · Talgat Inerbaev · Bernard Kirtman · Feng Long Gu

Received: 22 July 2011 / Accepted: 22 September 2011 / Published online: 18 October 2011

Abstract An ab initio study of the effect on nonlinear optical (NLO) properties of medium-size polymethineimine (PMI) chains caused by doping with an alkali metal atom along the backbone is presented. Both the electronic and (preliminary) vibrational static first hyperpolarizabilities are investigated. Doping leads to the injection of an excess electron into the PMI chain, which is accompanied by major enhancement of its NLO response. Along with the hyperpolarizability, other electronic and structural properties depend strongly upon the position of doping along the chain. The vibrational contribution is larger than the corresponding electronic one for most of the cases studied.

Keywords Nonlinear optical properties · Polymethineimines · Dopant effect · Hyperpolarizabilities

Dedicated to Professor Akira Imamura on the occasion of his 77th birthday and published as part of the Imamura Festschrift Issue.

Electronic supplementary material The online version of this article (doi:10.1007/s00214-011-1058-x) contains supplementary material, which is available to authorized users.

L. Z. Kang · T. Inerbaev · F. L. Gu (✉)
Center for Computational Quantum Chemistry,
South China Normal University, Guangzhou 510631, China
e-mail: gu@scnu.edu.cn; fenglonggu@gmail.com

B. Kirtman
Department of Chemistry and Biochemistry,
University of California, Santa Barbara, CA 93106-9510, USA
e-mail: kirtman@chem.ucsb.edu

F. L. Gu
CREST, Japan Science and Technology Agency(JST),
4-1-8 Honchou, Kawaguchi, Saitama 332-0012, Japan

1 Introduction

In recent years, a great deal of work has been devoted to study the nonlinear optical (NLO) properties for many different types of material [1–5] due to potential applications in photonic and electro-optic devices that could be used, for example, in optical data storage, optical communication, and optical limiting [3, 4, 6–8]. Some investigations of second-order NLO properties (i.e., first hyperpolarizabilities) have concentrated on systems where the presence of "excess" electrons leads to large NLO response [9–12]. Typically the systems of interest in this regard are alkalides [13] and electrides [14, 15] that have been synthesized in the laboratory in recent years.

Previous studies have demonstrated that a large static first hyperpolarizability, β_0, [9–11, 16–18] can be induced in conjugated organic chains by capping on one end with an alkali atom. This results from combining asymmetry with delocalization of the electronic charge transferred to the conjugated moiety. Alkali doping can also enhance the second hyperpolarizability (γ) as shown by Champagne et al. [17] and Spassova et al. [18]. They studied polyacetylene (PA) oligomers doped either at a single site at the chain center or uniformly along the conjugated backbone; both electronic and vibrational hyperpolarizabilities were considered. In Ramırez-Solıs et al. [19], a comparison was made between Li and Na dopant. The most significant difference was the binding energies, and the appearance of a narrow isolated unoccupied band within the PA π–π^* gap in the case of the Na dopant.

In this paper, we investigate a case that combines some key features of the studies just described, but differs significantly from each of them. In particular, we consider Me-doping (Me = Li, Na, K) at a position along the backbone (rather than at the end) of a quasilinear

π-conjugated H–[C(H)=N]$_n$–H polymethineimine (PMI) chain. Unlike PA the monomeric units of PMI are asymmetric and we, therefore, consider β as opposed to γ. Although we are primarily interested here in the electronic hyperpolarizability, a preliminary assessment of the pure vibrational contribution to this property will be made as well. For asymmetric chains, the effect of doping near one end or the other can make a large difference. Thus, we examine the site dependence at both ends and at the chain center. In order to assess trends with increasing chain length, the cases $n = 4$, 6, 8 and 10 are studied. It turns out that the variation of the hyperpolarizability as a function of chain length is very different from that obtained previously for (HCN)$_n$··· Li [9]. The effect of alkali doping is analyzed in terms of doping-induced changes in molecular geometry as well as the electronic charge/spin distribution along the chain.

2 Computational details

Our original intent was to carry out calculations entirely at the UMP2 level for the doublet systems of interest here. However, in order to reduce computation time, we opted for UB3LYP geometry optimizations instead. Initial test calculations revealed that there are not large structural differences between UMP2 and UB3LYP. Furthermore, the differences between UB3LYP and ROB3LYP were found to be very small (see Table 3 in Supporting Information) indicating that the effect of spin contamination on the UB3LYP geometries is negligible. As far as accuracy is concerned, the existing evidence indicates no strong preference for one of these methods (i.e., UMP2 or UB3LYP) over the other. Thus, stable structures with all real frequencies were obtained using UB3LYP/6-31+G(d) with a tight convergence threshold.

Subsequent to the geometry optimizations, it was found that spin-unrestricted methods are inadequate for determining the first hyperpolarizability, although they are satisfactory for geometry optimization. As seen in the Supporting Information trial, calculations gave very large differences between UMP2 and ROMP2 (as well as UHF and ROHF) values for this property. These differences are substantially reduced in corresponding B3LYP calculations (see Supporting Information). However, it is well-known that conventional DFT methods are unsuitable for describing the chain length dependence of the hyperpolarizability in conjugated systems [20, 21], which is one of the issues we wished to explore. Hence, the static electronic first hyperpolarizabilities, β_0 (see Eq. 4) were evaluated at the ROMP2/6-31+G(d) level by means of the finite field approach. In support of this approach, we note that, for the smallest chain considered, the ROMP2 and ROB3LYP values turned out to be similar (see Supporting Information for 6-31G(d) results). Moreover, a comparison of ROMP2 with ROCCSD showed little effect due to introducing single excitations.

The choice of the 6-31+G(d) basis set was based on a recent recommendation in favor of its use for estimating correlated NLO properties of medium-size systems [22]. In test calculations, we found that the value of $\beta_{0,-}$ for Li(L_1)@(PMI)$_4$, (L_1 indicates the far left backbone position; see Fig. 1) obtained at the ROMP2/6-31+G(d) and ROMP2/6-31++G(d, p) levels of theory differ by <1% (See Table 2S of Supporting Information). Thus, we concluded that the 6-31+G(d) basis is sufficient to evaluate the electronic first hyperpolarizabilities.

The static electric dipole properties are defined by a Taylor series expansion of the energy as a function of an applied electric field [23, 24]:

$$E = E^0 - \mu_i F_i - \frac{1}{2!}\alpha_{ij}F_iF_j - \frac{1}{3!}\beta_{ijk}F_iF_jF_k\ldots \quad (1a)$$

In Eq. 1, E^0 is the zero field molecular energy, F_i is the component of the field along the ith Cartesian direction and the Einstein summation convention has been employed. The quantities μ_i are the components of the dipole moment whereas α_{ij} and β_{ijk} are the components of the polarizability and first hyperpolarizability tensors, respectively. Within the Born–Oppenheimer approximation, one may separate electronic and pure vibrational contributions to the (hyper)polarizability [25]; both are determined in this paper.

As a first step, the α_{ii} values for Me@(PMI)$_n$ (Me = Li, Na, K; $n = 4$, 6, 8, 10) were evaluated analytically by the ROMP2 method. Then, the first hyperpolarizabilities of interest (see below) were determined by numerical

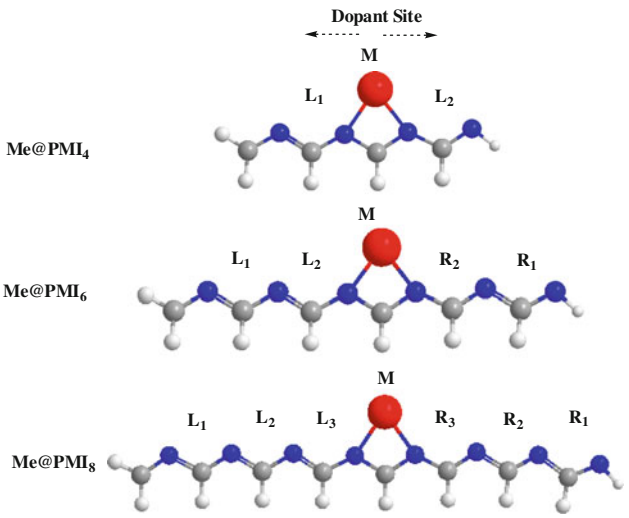

Fig. 1 Schematic geometry of the various isomers of Me@(PMI)$_n$ (Me = Li, Na, K; $n = 4$, 6, 8). *Blue* atoms are N, *light gray* atoms are H, *dark gray* atoms are C, and *pink* atoms are alkali atoms

Table 1 Properties of doped PMI chains ($n = 4, 6, 8$) including (a) bond lengths (in Å) at the site (see Fig. 2 for definitions), (b) relative energies (kcal/mol) for different sites and different alkali atom dopant, (c) NPA charge q (a.u.) on alkali atom and (d) spin density ($n = 4, 6, 8$) on alkali atom

	R (1)	R (2)	R_a (Me–N)	R_b (Me–N)	BLA	Relative Energy	q (Li)
$Li(L_1)@PMI_4$[b]	0.710 (0.738)[a]	0.713 (0.678)	1.055	1.007	−0.003 (0.060)	5.416	0.86
$Li(M)@PMI_4$	0.706 (0.735)	0.706 (0.678)	1.035	1.022	−0.001 (0.057)	0.000	0.85
$Li(R_1)@PMI_4$	0.712 (0.740)	0.698 (0.675)	1.020	1.027	0.015 (0.065)	0.611	0.86
$Na(L_1)@PMI_4$	0.710	0.711	1.256	1.176	−0.001	5.489	0.90
$Na(M)@PMI_4$	0.705	0.705	1.215	1.200	0.000	0.000	0.89
$Na(R_1)@PMI_4$	0.712	0.696	1.188	1.215	0.016	0.924	0.89
$K(L_1)@PMI_4$	0.710	0.710	1.512	1.368	0.000	5.153	0.93
$K(M)@PMI_4$	0.705	0.704	1.421	1.403	0.001	0.000	0.93
$K(R_1)@PMI_4$	0.713	0.695	1.381	1.435	0.018	1.414	0.94
$Li(L_1)@PMI_6$	0.713 (0.737)	0.713 (0.680)	1.064	1.012	−0.0004 (0.057)	8.378	0.87
$Li(M)@PMI_6$	0.704 (0.731)	0.707 (0.681)	1.041	1.032	−0.003 (0.049)	0.000	0.87
$Li(R_1)@PMI_6$	0.715 (0.739)	0.694 (0.676)	1.023	1.036	0.023 (0.063)	1.120	0.87
$Na(R_1)@PMI_6$	0.716	0.692	1.023	1.192	0.024	–	0.90
$K(R_1)@PMI_6$	0.717	0.691	1.384	1.457	0.026	–	0.94
$Li(L_1)@PMI_8$	0.714 (0.736)	0.713 (0.680)	1.070	1.015	0.001 (0.056)	9.648	0.87
$Li(M)@PMI_8$	0.703 (0.728)	0.707 (0.683)	1.044	1.038	−0.004 (0.045)	0.000	0.87
$Li(R_1)@PMI_8$	0.717 (0.738)	0.692 (0.676)	1.026	1.040	0.026 (0.063)	1.183	0.87

The BLA = R(1)−R(2) (Å) is the bond length alternation at the dopant site

[a] The value in parentheses is the CN bond length for undoped PMI chains

[b] The L_1, M and R_1 dopant sites are shown in Fig. 1

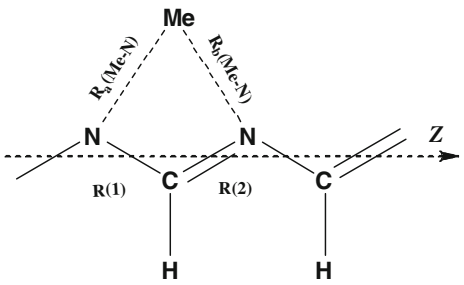

Fig. 2 Bond length parameters that characterize the dopant site for Me@$(PMI)_n$. The longitudinal z axis connects the carbon atoms at either end of the chain and the complex lies in the xz plane

differentiation [26–28] of α_{ii} (i = x, y, z) with respect to a field in the longitudinal direction (z) as follows:

$$\beta_{iiz} = \frac{\alpha_{ii}(+F_z) - \alpha_{ii}(-F_z)}{2F_z}, \quad i = x, y, z \tag{1b}$$

Here the longitudinal z axis is determined by the line connecting the first and last carbon atoms of the chain (the complex lies in the xz plane). From preliminary calculations (see Supporting Information), it was found that an applied field of 0.0001 a.u. led to stable derivatives at zero field as desired; hence, that value was employed in Eq. 1b. Instead of comparing individual components, it will often be convenient to use the combinations:

$$\mu_0 = \left(\mu_x^2 + \mu_y^2 + \mu_z^2\right)^{1/2} \tag{2}$$

$$\alpha_0 = \frac{1}{3}\left(\alpha_{xx} + \alpha_{yy} + \alpha_{zz}\right) \tag{3}$$

$$\beta_0 = \beta_{iiz} = \frac{3}{5}\left(\beta_{xxz} + \beta_{yyz} + \beta_{zzz}\right), \quad i = x, y, z \tag{4}$$

A preliminary estimate for the static vibrational first hyperpolarizability was made for the $n = 4$ chain at the double harmonic level of approximation. ROMP2 computations are too time-consuming to be used for this purpose and the UMP2 method was employed instead. In order to roughly compensate for the effect of spin contamination, we scaled the UMP2 vibrational hyperpolarizability using an appropriate ROMP2/UMP2 ratio of electronic properties. The ratio, shown in Eq. 5, was dictated by the fact that the vibrational first hyperpolarizability is determined by the product of an electronic dipole term and an electronic linear polarizability term (see Eq. 6 below):

$$\frac{\beta_{zzz,\mathrm{vib}}^{\mathrm{ROMP2}}}{\beta_{zzz,\mathrm{vib}}^{\mathrm{UMP2}}} = \frac{\alpha_{zz,\mathrm{el}}^{\mathrm{ROMP2}} \cdot \mu_{z,\mathrm{el}}^{\mathrm{ROMP2}}}{\alpha_{zz,\mathrm{el}}^{\mathrm{UMP2}} \cdot \mu_{z,\mathrm{el}}^{\mathrm{UMP2}}} \tag{5}$$

Note that this treatment is used only for the pure longitudinal component. However, we shall see that the hyperpolarizability defined in Eq. 4 is dominated by this

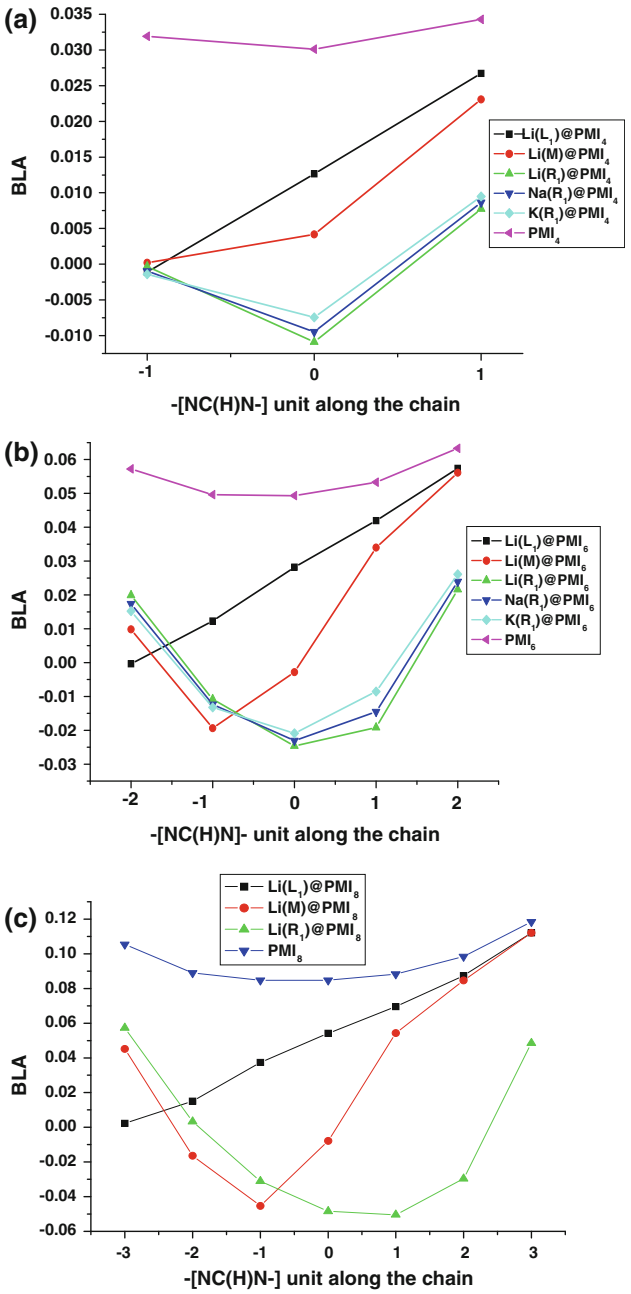

Fig. 3 BLA (Å) as a function of position for doped and undoped PMI chains. The position "0" refers to the –[NC(H)N]– unit at the middle site; "1" to the next unit to the right, "−1" to the opposite side and so forth

component (at least for the electronic contribution), so that $\beta_0 \approx (3/5)\beta_{zzz}$. As required for the consistency, the vibrational normal coordinates and frequencies that enter into the expression for the vibrational hyperpolarizability (see Eq. 6 below) were evaluated at the UMP2/6-31+G(d) optimized geometry. On the other hand, the electronic properties, which are not as sensitive to structure, were those calculated at the UB3LYP/6-31+G(d) geometry. According to the double harmonic approximation, the static (unscaled) vibrational first hyperpolarizability (pure longitudinal component) is given by [29]:

$$\beta^{v}_{zzz} = [\mu\alpha] = 3\sum_{a}\frac{1}{\omega_a^2}\left(\frac{\partial\mu^e_z}{\partial Q_a}\right)_0\left(\frac{\partial\alpha^e_{zz}}{\partial Q_a}\right)_0, \quad (6)$$

where Q_a is the normal coordinate for the vibrational motion with circular frequency $\omega_a = 2\pi\upsilon_a$; the subscript 0 on the partial derivatives indicates the equilibrium nuclear configuration. In utilizing Eq. 6, the partial derivatives were calculated numerically. Obviously, our results for the vibrational hyperpolarizabilities must be regarded with caution, not only because anharmonic effects have been omitted but also because of the approximations (i.e., scaling) made within the double harmonic treatment.

Finally, all calculations were performed with the GAUSSIAN 03 program package [30]. Net atomic charges were obtained using the natural population analysis (NPA) included in the natural bond orbital algorithm [31, 32]. The plots of molecular orbitals were generated with the GaussView program (Gaussian, Inc., Pittsburgh, PA) [33].

3 Results and discussion

3.1 Geometrical characteristics and atomic charge/spin populations of Me@H–[C(H)N]$_n$–H (Me = Li, Na, K; n = 4, 6, 8)

The schematic geometrical structure of the various isomers of Me-doped PMI is shown in Fig. 1. As seen in the figure, the alkali atom is located at a site where it forms a quasi-symmetrical 3-center bond with two neighboring N atoms. There are $n-1$ dopant sites for each chain. In order to get a feeling for the range of behavior, we decided to focus on the left-most (carbon end; L_1-site), right-most (nitrogen end; R_1-site) and middle (M-site) position. For Li-doping, the M-site is the most stable among these structures, followed by the R_1-site with a difference on the order of 1 kcal/mol (see Table 1). This energy difference increases with chain length but appears to be nearly converged at about 1.2 kcal/mol at $n = 8$. For Li-doping at the L_1-site, the energy differences are much larger.

The bond lengths that characterize the dopant site are collected in Table 1. In the table R(1) and R(2) (see Fig. 2) refer to the N–C bond (single in undoped PMI) and C–N bond (double in undoped PMI) located, respectively, at the left- and right-hand sides of the dopant site. Note that the bond length alternation (BLA = R(1)–R(2)) at every –[NC(H)N]– unit is reduced—substantially in most instances (see Fig. 3)—from what it is at the same site of the undoped PMI chain. Compared to C=N bonds in the corresponding undoped PMI chain, the R(2) distance at the

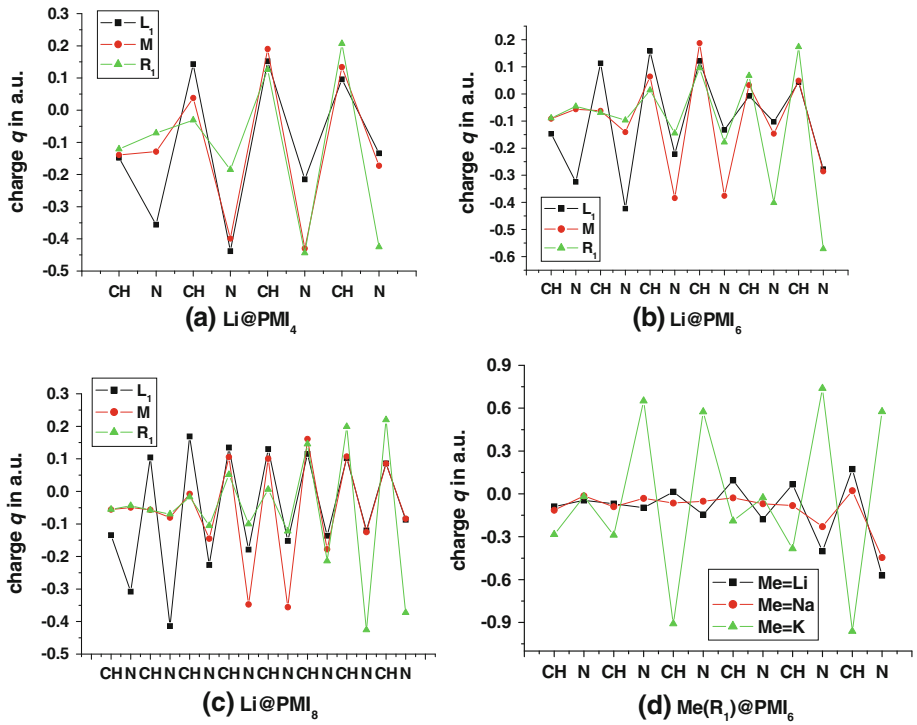

Fig. 4 Net electronic charge transferred to (or from) backbone N atoms and C(H) groups due to (1) Li-doping of $(PMI)_n$ chains : **a** $n = 4$, **b** $n = 6$ and **c** $n = 8$; (2) different alkali atoms doping at the R_1-site; **d** $n = 6$ with Me = Li, Na, and K

dopant sites is elongated (0.035–0.023 Å ($n = 4$)), 0.033–0.018 Å ($n = 6$) and 0.033–0.016 Å ($n = 8$)) in Li@$(PMI)_n$, while the R(1) bonds are shortened (0.028–0.029 Å ($n = 4$), 0.024–0.027 Å ($n = 6$) and 0.025–0.021 Å ($n = 8$)) (See Table 1) compared to C–N bonds in the corresponding undoped PMI chain. In fact, the R(1) and R(2) bond lengths are essentially the same for doping at the M- and L_1-sites, whereas a difference of 0.015–0.026 Å persists at the R_1-site. The BLA is larger at the R_1-site for the undoped chains as well, but the difference between L_1 and R_1 is smaller than the above by a factor of 3–4.

As a function of position along the chain, the BLA exhibits a strong asymmetry. The resulting patterns, particularly for the M- and R_1-sites, are quite different from what one might have expected from polaron-like behavior. For the L_1-site, Fig. 3 shows that the doping eliminates the BLA at that site. Then, the BLA increases linearly as one proceeds toward the opposite end of the chain, in accord with a steady diminution of the doping effect. For $n = 8$, the doped and undoped BLA at the far right-hand end are essentially the same. However, the pattern is quite different for doping at the R_1-site. In that case, the BLA is reduced at the site, though maybe not as much as one might have anticipated from L_1—doping—with increasing chain length it levels off to roughly 50% of the undoped value. As one progresses toward the opposite chain end, instead of the BLA being restored, it is reduced further; indeed, there is a sign change, with a maximum magnitude near the center of the chain. Beyond the chain center, the BLA increases back toward the value at the dopant site. Doping at the chain center reflects the effect of doping at either end. Surprisingly, perhaps, the BLA pattern on the right-hand side of the chain follows that for doping at the L_1-site while the pattern on the left-hand side of the chain follows that for doping at the R_1-site.

For alkali-atom doping at the different sites, the two Me–N distances show some noteworthy trends (see Table 1). The left-hand bond, which is substantially the longer of the two at the L_1-site, decreases in length as the doping site is changed from L_1 to M to R_1, while the shorter right-hand bond continuously increases. In fact, there is a switch-over between the M- and R_1-sites, i.e., the right-hand bond becomes the longer of the two. In addition, the mean Me–N distance increases with increasing alkali atomic number from roughly 1.0 Å for Li(R_1)@PMI_n to 1.1–1.2Å for Na(R_1)@PMI_n to 1.4 Å K(R_1)@PMI_n. These distances are much shorter than the sum of the ionic radius of the alkali and the covalent radius of nitrogen. It will be shown in the following that both the dopant site and the particular alkali atom are important factors affecting the value of the hyperpolarizability.

As indicated in Fig. 1, the chains are bent. We find that the bend angle, θ, as defined by the intersection of the lines

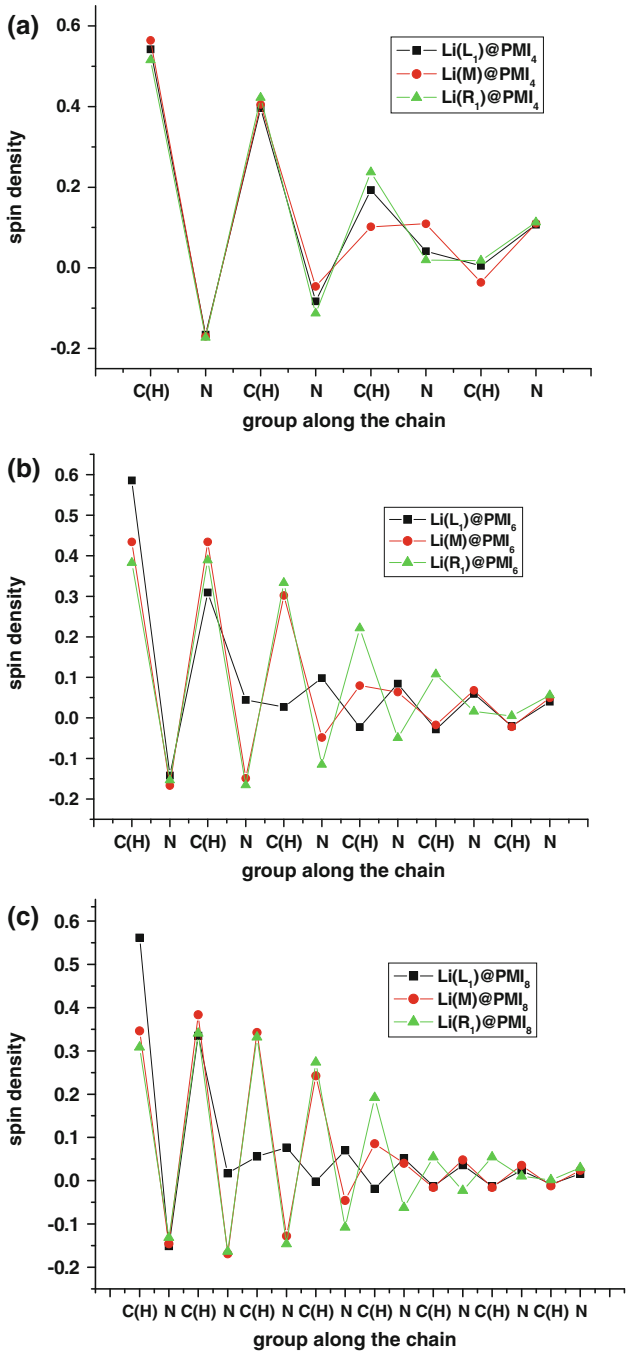

Fig. 5 Spin density contribution of backbone atoms for Li-doped PMI chains **a** $n = 4$, **b** $n = 6$ and **c** $n = 8$

passing through the midpoints of the two terminal C=N bonds [17] at either end is 13.1° (22.44°) for the $n = 4$ (6) undoped PMI oligomer (not shown). The effect of doping for different alkali atoms (Li, Na and K) at the R_1 position, for example, is to decrease this angle to 4.05°, 4.13° and 5.06° for $n = 4$ (11.09°, 14.36° and 14.95° for $n = 6$).

As determined from a natural population analysis (NPA) [32] of ROMP2/6-31+G(d) results, doping a PMI chain with an Li atom leads to essentially the same total electronic charge transfer (0.85e–0.87e) regardless of the doping site or the chain length. There is a big and significant increase with the atomic number of the alkali atom. Figure 4 shows a clear oscillatory behavior in the vicinity of the dopant site where the electronic charge is transferred to the nitrogen atoms while the intervening C(H) units (as is customary the C and H charges have been combined) are either positive or much less negatively charged. These oscillations are damped as one proceeds along the chain away from the dopant site and, typically, will switch so that C(H) becomes the charge transfer site. Such damped charge oscillations are in accord with what one might expect from polaron formation.

The excess spin for Li-doping, obtained from ROMP2 calculations, differs from the charge transfer in that it lies entirely on the chain backbone. Again, there is a clear damped oscillatory behavior. However, in contrast with charge transfer, we see in Figs. 5, 6 that, regardless of dopant site, the maximum spin density resides at the left-hand end of the chain. Moreover, the excess spin is located on the C(H) groups rather than on the N atoms. For doping at the L_1-site, the magnitude of the spin density on the C(H) at the left-hand end of the chain remains close to 0.6e for all chain lengths, but this value falls off rapidly for the other two doping sites from about 0.55e for $n = 4$ to about 0.35e for $n = 8$. The oscillations are also damped most rapidly for doping at the L_1-site (see, particularly, the $n = 6$ and $n = 8$ chains).

Evidently, any interpretation of what happens to the alkali valence electron as a result of the doping process depends strongly upon whether that interpretation is based on charge or spin. Alkali doping of PMI oligomers is a complex process, in which electronic charge is transferred primarily to N atoms near the dopant site and the conjugation (i.e., BLA) at that site is strongly reduced, whereas spin polarization is transmitted to the C(H) group at the left-hand end of the chain. The asymmetry of the chain is reflected not only in the spin polarization but also in the stronger binding, larger BLA and greater charge localization at the R_1-site as opposed to the L_1-site.

3.2 Static electronic first hyperpolarizabilities of Me@PMI$_n$ (Me = Li, Na, K; $n = 4, 6, 8, 10$)

The ROMP2/6-31+G(d) static electronic hyperpolarizabilities of undoped PMI chains and PMI chains doped with a single alkali (Li, Na or K) atom, as calculated for different chain lengths, are given in Table 2. From this table, it can be seen that (i) alkali-atom doping enhances, or greatly enhances, the magnitude of β_0 for all chain lengths; (ii) the β_{zzz} component makes the dominant contribution to β_0; (iii) in general, (though not always) β_0 increases with chain length for Li-doping; (iv) R_1 doping sites give the

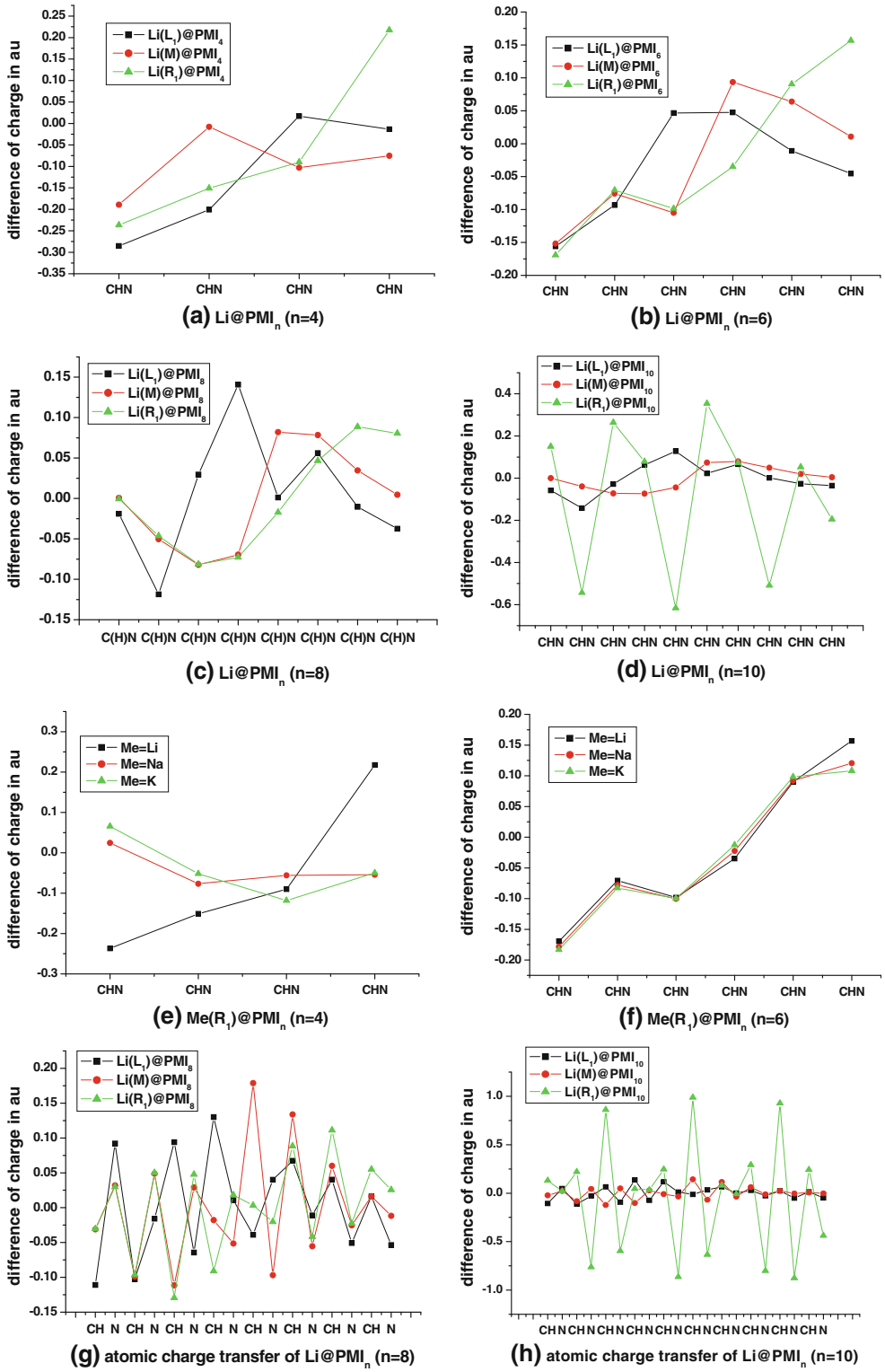

Fig. 6 Atomic charge differences between ground state and lowest excited state with oscillator strength $f_0 > 0.1$ for Me@PMI$_n$ chains (Me = Li, Na, K; $n = 4, 6, 8, 10$)

largest hyperpolarizability values as compared to other sites and undoped PMI chains. These are the two most important doping sites since they are the most stable. There are two apparently exceptional results in the table. They occur for the $n = 8$ chain at the M-site (large negative β_0) and at the R1-site (small α_0). In either case, the

Table 2 Electronic dipole moment μ_0, static average polarizability (α_0; see Eq. 3) and static first hyperpolarizability $\beta_{iiz} = \beta_0$ (Eq. 4), as well as the individual components that contribute to the latter property

	μ_0	α_0	β_{xxz}	β_{yyz}	β_{zzz}	β_0
PMI_4	3.000	93.45	140	10	955 (0)	663 (0)
$Li(L_1)@PMI_4$	2.259	134.47	−92	−450	2,600 (0)	1,235 (0)
$Li(M)@PMI_4$	0.623	149.52	−349	−466	−6,709 (0)	−4,515 (0)
$Li(R_1)@PMI_4$	2.065	118.13	555	−17	4,234 (1)	2,573 (1)
$Na(L_1)@PMI_4$	2.501	139.34	−85	−470	2,541 (0)	1,192 (0)
$Na(M)@PMI_4$	0.832	153.51	−9	−349	9,785 (0)	5,657 (0)
$Na(R_1)@PMI_4$	2.288	84.00	344	45	1,922 (1)	1,177 (1)
$K(L_1)@PMI_4$	2.865	147.69	59	−381	3,012 (0)	1,614 (0)
$K(M)@PMI_4$	1.609	156.73	−36	−428	9,131 (0)	5,200 (0)
$K(R_1)@PMI_4$	2.687	126.41	301	−417	−1,090 (2)	−6,545 (1)
PMI_6	4.702	164.86	286	25	3,412 (0)	2,234 (0)
$Li(L_1)@PMI_6$	5.122	242.92	−1,018	−1,411	1,670 (1)	8,563 (0)
$Li(M)@PMI_6$	1.690	244.16	38	−161	7,120 (0)	4,198 (0)
$Li(R_1)@PMI_6$	3.480	284.14	−100	−295	2,219 (1)	1,308 (1)
$Na(L_1)@PMI_6$	5.366	254.25	−58	−557	2,064 (1)	1,202 (1)
$Na(M)@PMI_6$	0.912	248.92	117	−99	6,982 (0)	4,200 (0)
$Na(R_1)@PMI_6$	3.969	280.16	250	−91	1,681 (1)	1,018 (1)
$K(R_1)@PMI_6$	4.527	281.88	−62	−180	1,069 (1)	6,270 (0)
PMI_8	3.32	251.94	461	−6	8,410 (0)	5,319 (0)
$Li(L_1)@PMI_8$	8.123	378.64	890	−995	5,205 (1)	3,117 (1)
$Li(M)@PMI_8$	3.856	343.15	62	−230	−2,967 (2)	−1,781 (2)
$Li(R_1)@PMI_8$	5.507	260.57	−332	481	2,532 (2)	1,520 (2)
PMI_{10}	8.32	352.19	748	49	1,625 (1)	1,023 (1)
$Li(L_1)@PMI_{10}$	11.25	536.47	788	−450	1,107 (2)	6,664 (1)
$Li(M)@PMI_{10}$	4.470	561.91	782	57	1,531 (2)	9,235 (1)
$Li(R_1)@PMI_{10}$	7.853	654.48	4,863	−1,172	4,130 (2)	2,500 (2)

All quantities are in a.u., and the integer in parentheses indicates multiplication by that power of 10

[a] $1au = 8.63922 \times 10^{-33}$ esu

corresponding plot of α_0 *vs.* F_z (see Eq. 1b and Supporting Information) exhibits exceptional behavior that we cannot explain as yet.

It is of interest to compare the values obtained here to other systems with large β_0. For the excess electron compound, Li^+TCNQ^- the calculated β_0 (determined using ROMP2 with a somewhat larger basis set than we have employed) is 17,086 a.u. [34]. This is considerably smaller in magnitude than the value for $Li@PMI_8$ (for example) at all doping sites, but especially R_1 and M. On the other hand, for donor–acceptor polyene systems [35], β_0 values ranging up to 153,000 a.u. have been obtained. The latter value is about the same as for Li-doping of the $n = 8$ chain at the R_1- and M-sites. This stimulated us to consider the $n = 10$ chain, for which the last three values in Table 2 have been obtained. We note that the value of β_0 at the R_1-site is about 1.5 times larger than that calculated for the $n = 8$ chain. How much further that value will increase for Li-doped PMI oligomers with $n > 10$ remains to be seen.

3.3 Preliminary assessment of pure vibrational β

The pure electronic contribution to the static first hyperpolarizability (β^e) is obtained with the nuclei frozen at the optimized geometry. It is now well-known [17, 36, 37] that there is also a pure vibrational contribution to the first hyperpolarizability, β^v, which may be associated with the relaxation of the geometry induced by the polarizing field. At the lowest level of the treatment, β^v can be estimated in the double harmonic approximation given by Eq. 6. Even at the double harmonic level, the calculations can be tedious because it is necessary to determine the harmonic vibrational force constants. Hence, we have considered only the $n = 4$ chain. Our calculated values of β^v_{zzz}, and for comparison purposes β^e_{zzz}, are reported in Tables 3, 4. Both the scaled and unscaled values of β^v_{zzz} are shown in order to see the effect of scaling. Even though we suspected that the vibrational contributions might be important, their very large size is striking. They range from roughly the same

Table 3 Lowest excited state of Me@PMI_n (Me = Li, Na, K; $n = 4, 6, 8, 10$) with oscillator strength $f_0 > 0.1$ as determined by TDDFT (B3LYP/6-31+G(d)

	Excited state	$\Delta E_{(eV)}$	$\Delta\mu_z$	f_0	Transition
PMI_4					
$Li(L_1)@PMI_4$	3rd	3.415	1.20	0.1205	Homo-lumo + 3
$Li(M)@PMI_4$	5th	3.665	1.179	0.1248	Homo-lumo + 5
$Li(R_1)@PMI_4$	1st	2.553	1.431	0.1280	Homo-lumo + 1
$Na(R_1)@PMI_4$	2nd	2.574	1.385	0.1210	Homo-lumo + 1
$K(R_1)@PMI_4$	2nd	2.568	1.329	0.111	Homo-lumo + 2
PMI_6					
$Li(L_1)@PMI_6$	2nd	2.813	3.367	0.7813	Homo-lumo
$Li(M)@PMI_6$	1st	2.171	1.772	0.167	Homo-lumo
$Li(R_1)@PMI_6$	1st	2.043	2.510	0.3154	Homo-lumo
$Na(R_1)@PMI_6$	1st	2.059	2.456	0.3042	Homo-lumo + 1
$K(R_1)@PMI_6$	1st	2.066	2.386	0.2881	Homo-lumo + 1
PMI_8					
$Li(L_1)@PMI_8$	2nd	2.448	3.616	0.7842	Homo-lumo
$Li(M)@PMI_8$	1st	1.886	2.760	0.352	Homo-lumo
$Li(R_1)@PMI_8$	1st	1.685	3.596	0.5338	Homo-lumo
PMI_{10}					
$Li(L_1)@PMI_{10}$	2nd	2.206	3.433	0.637	Homo-lumo
$Li(M)@PMI_{10}$	1st	1.667	3.849	0.605	Homo-lumo
$Li(R_1)@PMI_{10}$	1st	1.429	4.569	0.731	Homo-lumo

ΔE is the transition energy, and $\Delta\mu_z$ is the difference of dipole moment between the ground state and the crucial excited states

Table 4 Double harmonic vibrational contribution β^v (a.u.) to the longitudinal component of the static first hyperpolarizability for alkali-doped PMI_4 chains

	β^e_{zzz}	β^v_{zzz}(scaled; Eq. 5)	β^v_{zzz}(UMP2)
$Li(L_1)@PMI_4$	2,600 (0)	−2,982 (4)	1,573 (3)
$Na(L_1)@PMI_4$	2,541 (0)	−4,044 (4)	−1,542 (3)
$K(L_1)@PMI_4$	3,012 (0)	1,004 (3)	1,455 (2)
$Li(M)@PMI_4$	−6,709 (0)	21 (0)	3.9 (0)
$Na(M)@PMI_4$	9,785 (0)	190 (0)	12.2 (0)
$K(M)@PMI_4$	9,131 (0)	1,262 (3)	7,328 (2)
$Li(R_1)@PMI_4$	4,234 (1)	1,370 (2)	2,122 (2)
$Na(R_1)@PMI_4$	1,922 (1)	1,767 (2)	5,569 (2)
$K(R_1)@PMI_4$	−1,092 (2)	−3,114 (2)	−5,099 (2)

These results were obtained using Eq. 5 for the scaled ROMP2 value and Eq. 6 for the UMP2 value as described in the text. In either case, the 6-31+G(d) basis was employed. The corresponding electronic hyperpolarizability is given for comparison, and the number in parentheses is the power of 10 by which the reported value must be multiplied

magnitude as the electronic term to more than four orders of magnitude larger. This indicates that it is essential that they be taken into account for the type of system studied here. The primary reason for the very large values is that the vibrational potential is quite shallow. Consequently, the anharmonic contributions need to be considered as well. Fortunately, there are so-called nuclear relaxation methods [38] for doing so that are computationally feasible and will be the subject of future studies.

4 Conclusions

The results of ab initio simulation of both first static electronic and vibrational hyperpolarizabilities of alkali-metal doped medium-sized PMI chains are presented. Dependences of NLO properties on both dopant site with respect to polymer chain and its kind are considered. It is found that alkali-metal doping leads to ground-state electron transfer from metal atom to the PMI chain. The value

of the transferred charge is almost independent, while the distribution of the transferred charge along the chain is strongly dependent on the position of alkali-atom doping. This charge transfer is accompanied with simultaneous decrease in BLA in the vicinity of doping atom compared to that of undoped PMI chain. These effects lead to significant increase in first static hyperpolarizability that is caused by PMI backbone-to-doping atom ground-to-excited charge transfer and critically depends on the position of dopant on the PMI chain. It is also shown that the vibrational contribution on hyperpolarizability by double harmonic approximation is larger than the corresponding electronic one in all considered cases except the case of $Me(L_1)@PMI_4$ (Me = Li and Na) configuration and almost independent on the kind of doping atoms. This indicates that the motion of PMI's backbone atoms give the main contribution in vibrational hyperpolarizability.

Acknowledgments We are grateful to the financial support from the National Science Foundation of China (NO.738196). All the calculations were carried out on the Linux cluster systems in our laboratory at SCNU.

References

1. Eaton DF (1991) Nonlinear optical materials. Science 253:281–287
2. Cheng WD, Xiang KH, Pandey R, Pernisz UC (2000) Calculations of linear and nonlinear optical properties of H–Silsesquioxanes. J Phys Chem B 104:6737–6742
3. Geskin VM, Lambert C, Bredas JL (2003) Origin of high second- and third-order nonlinear optical response in ammonio/borato diphenylpolyene zwitterions: the remarkable role of polarized aromatic groups. J Am Chem Soc 125:15651–15658
4. Nakano M, Fujita H, Takahata M, Yamaguchi K (2002) Theoretical study on second hyperpolarizabilities of phenylacetylene dendrimer: toward an understanding of structure–property relation in NLO responses of fractal antenna dendrimers. J Am Chem Soc 124:9648–9655
5. Ichida M, Sohda T, Nakamura A (2000) Third-order nonlinear optical properties of C60 CT complexes with aromatic amines. J Phys Chem B 104:7082–7084
6. Marder SR, Cheng LT, Tiemann BG, Friedli AC, Blancharddesce M, Perry JW, Skindhoj J (1994) Large first hyperpolarizabilities in push-pull polyenes by tuning of the bond length alternation and aromaticity. Science 263:511–514
7. Marder SR et al (1997) Large molecular third-order optical nonlinearities in polarized carotenoids. Science 276:1233–1236
8. Kirtman B, Champagne B, Bishop DM (2000) Electric field simulation of substituents in donor–acceptor polyenes: a comparison with ab initio predictions for dipole moments, polarizabilities, and hyperpolarizabilities. J Am Chem Soc 122:8007–8012
9. Chen W, Li ZR, Wu D, Li RY, Sun CC (2005) Theoretical investigation of the large nonlinear optical properties of $(HCN)_n$ clusters with Li atom. J Phys Chem B 109:601–608
10. Chen W, Li ZR, Wu D, Li Y, Sun CC, Gu FL (2005) The structure and the large nonlinear optical properties of Li@Calix[4]pyrrole. J Am Chem Soc 127:10977–10981
11. Chen W, Li ZR, Wu D, Li Y, Sun CC, Gu FL, Aoki Y (2006) Nonlinear optical properties of alkalides Li+(calix[4]pyrrole)M- (M=Li, Na, and K): alkali anion atomic number dependence. J Am Chem Soc 128:1072–1073
12. Jing YQ, Li ZR, Wu D, Li Y, Wang BQ, Gu FL, Aoki Y (2006) Effect of the complexant shape on the large first hyperpolarizability of alkalides Li+(NH3)4 M−. Chem Phys Chem 7:1759–1763
13. Wagner MJ, Dye JL (1996) In: Gokel GW (ed) Molecular recognition: receptors for cationic guests, vol 1. Pergamon, Oxford, pp 477–510
14. Ichimura AS, Dye JL, Camblor MA, Villaescusa LA (2002) Toward inorganic electrides. J Am Chem Soc 124:1170–1171
15. Dye JL (1997) Electrides: from 1D heisenberg chains to 2D pseudo-metals†. Inorg Chem 36:3816–3826
16. Xu HL, Wang FF, Li ZR, Wang BQ, Wu D, Chen W, Yu GT, Gu FL, Aoki Y (2009) The nitrogen edge-doped effect on the static first hyperpolarizability of the supershort single-walled carbon nanotube. J Comput Chem 30:1128–1134
17. Champagne B, Spassova M, Jadin J, Kirtman B (2002) Ab initio investigation of doping-enhanced electronic and vibrational second hyperpolarizability of polyacetylene chains. J Chem Phys 116:3935–3947
18. Spassova M, Champagne B, Kirtman B (2005) Large effect of dopant level on second hyperpolarizability of alkali-doped polyacetylene chains. Chem Phys Lett 412:217–222
19. Ramirez-Solis A, Kirtman B, Bernal-Jaquez R, Zicovich-Wilson C (2008) Periodic density functional theory calculations for Na-doped Quasi-one-dimensional polyacetylene chains. J Phys Chem C 112:9493–9500
20. Champagne B, Perpète EA, Van Gisbergen S, Baerends EJ, Snijders JG, Soubra-Ghaoui C, Robins K, Kirtman B (1998) Assessment of conventional density functional schemes for computing the polarizabilities and hyperpolarizabilities of conjugated oligomers: An ab initio investigation of polyacetylene chains. J Chem Phys 109:10489–10498
21. Champagne B, Perpète EA, Jacquemin D, Van Gisbergen S, Baerends E, Soubra-Ghaoui C, Robins K, Kirtman B (2000) J Phys Chem A 104:4755–4763
22. Torrent-Sucarrat M, Solà M, Duran M, Luis JM, Kirtman B (2003) Basis set and electron correlation effects on ab initio electronic and vibrational nonlinear optical properties of conjugated organic molecules. J Chem Phys 118:711–719
23. Buckingham AD (1967) Permanent and induced molecular moments and long-range intermolecular forces. Adv Chem Phys 12:107–142
24. Mclean AD, Yoshimine M (1967) Theory of molecular polarizabilities. J Chem Phys 47:1927–1935
25. Bishop D, Norman P (2001) Handbook of advanced electronic and photonic materials and devices, vol 9, HS Nalwa (ed), Academic, San Diego
26. Cohen HD, Roothaan CCJ (1965) Electric dipole polarizability of atoms by the Hartree-Fock method. I. Theory for closed - shell systems. J Chem Phys 43:S34–S39
27. Maroulis G (1991) Predicting partition coefficients for isomeric diastereoisomers of some tripeptide analogs. J Chem Phys 94:1182–1186
28. Kurtz HA, Stewart JJP, Dieter KM (1990) Calculation of the nonlinear optical properties of molecules. J Comput Chem 11:82–87
29. Champagne B, Kirtman B (1999) Vibrational versus electronic first hyperpolarizabilities of π-conjugated organic molecules: an ab initio Hartree–Fock investigation upon the effects of the nature of the linker. Chem Phys 245:213–216
30. Frisch MJ et al (2003) Gaussian 03, revision B03. Gaussian, Inc., Pittsburgh

31. Reed AE, Weinhold F (1983) Natural bond orbital analysis of near-Hartree–Fock water dimer. J Chem Phys 78:4066–4074
32. Reed AE, Weinstock RB, Weinhold F (1985) Natural population analysis. J Chem Phys 83:735–747
33. Dennington IIR, Todd K, Millam J, Eppinnett K, Hovell WL, Gilliland R (2003) GaussView, version 3.09. Semichem, Inc, Shawnee Mission
34. Li ZJ, Li ZR, Wang FF, Ma F, Chen MM, Huang XR (2009) The charge transfer anion-radical alkali-metal salts M(+)TCNQ(−) (M=Li, Na, K): The structures and static hyperpolarizabilities. Chem Phys Lett 468:319–324
35. BlanchardDesce M, Alain V, Bedworth PV, Marder SR, Fort A, Runser C, Barzoukas M, Lebus S, Wortmann R (1997) Large quadratic hyperpolarizabilities with donor–acceptor polyenes exhibiting optimum bond length alternation: correlation between structure and hyperpolarizability. Chem. 3:1091–1104
36. Perpete EA, Champagne B, Jacquemin D (2000) Electronic and vibrational first hyperpolarizabilities of polymethineimine oligomers. J Mol Struct-Theochem 529:65–71
37. Luis JM, Champagne B, Kirtman B (2000) Calculation of static zero-point vibrational averaging corrections and other vibrational curvature contributions to polarizabilities and hyperpolarizabilities using field-induced coordinates. Int J Quantum Chem. 80:471–479
38. Kirtman B, Luis JM (2008) Simple finite field nuclear relaxation method for calculating vibrational contribution to degenerate four-wave mixing. J Chem Phys 128:114101–114105